

DRIFT: Deep Reinforcement Learning for Intelligent Floating Platforms Trajectories

Matteo El-Hariry^{*1}, Antoine Richard^{*1}, Vivek Muralidharan¹, Barış Can Yalçın¹,
Matthieu Geist², Miguel Olivares-Mendez¹

Abstract—This investigation introduces a novel deep reinforcement learning-based suite to control floating platforms in both simulated and real-world environments. Floating platforms serve as versatile test-beds to emulate microgravity environments on Earth. Our approach addresses the system and environmental uncertainties in controlling such platforms by training policies capable of precise maneuvers amid dynamic and unpredictable conditions. Leveraging state-of-the-art deep reinforcement learning techniques, our suite achieves robustness, adaptability, and good transferability from simulation to reality. Our Deep Reinforcement Learning (DRL) framework provides advantages such as fast training times, large-scale testing capabilities, rich visualization options, and ROS bindings for integration with real-world robotic systems. Beyond policy development, our suite provides a comprehensive platform for researchers, offering open-access at <https://github.com/elharirymatteo/RANS/tree/ICRA24>.

I. INTRODUCTION

Across the globe, there has been exponential growth in the adoption of small satellites, including cubesats [1], [2]. Thanks to their cost-effectiveness, they are now extensively used for both commercial and scientific purposes. Consequently, several countries and their space administrations have actively invested in advancing small satellite technology over the past few decades. The surge in space missions is creating a growing demand to test and validate the flight software and hardware on the ground prior to employing them in space. These experiments aim to enhance the historically low success rates of missions in space [3].

Improving the reliability and autonomy of the motion systems plays a key role in boosting mission success. Currently, the primary approach to enhancing autonomous navigation and control of such systems involves conducting performance tests. These tests help understand essential parameters and their relationships within the control scheme involving different sensors and actuators. This knowledge is pivotal for the design and operation of these systems, contributing significantly to mission success rates. To emulate free-floating and free-flying satellite motion, a common solution is to use floating platforms: a rigid structure floating on top of an extremely flat and smooth surface using air bearings [4]. This allows 2D motions with very low friction, effectively replicating space-like conditions in a plane.

^{*}Equal contribution

¹Space Robotics (SpaceR) Research Group, SnT-University of Luxembourg, Campus Kirchberg 29, Avenue John F. Kennedy L-1855 Luxembourg {matteo.elhariry, antoine.richard, vivek.muralidharan, bariscan.yalcin, miguel.olivaresmendez}@uni.lu

²Matthieu Geist is with Google DeepMind mfgeist@google.com

The traditional methods of aerospace vehicle trajectory planning primarily rely on optimal control techniques, which involve the derivation of open-loop control solutions based on system models and predefined objectives. This approach is intricate and often necessitates specialized optimization software to find flight paths adhering to various constraints. However, as aerospace vehicles regularly encounter state disturbances and uncertainties, there is a growing need for more robust and adaptable control strategies.

In response to this challenge, this paper introduces a novel approach that harnesses the power of Deep Reinforcement Learning (DRL) to control a floating platform (FP) within a 2D environment. The utilization of DRL offers an alternative to the conventional deterministic and expert-driven control methods prevalent in aerospace trajectory planning. DRL involves a goal-oriented agent that interacts with its environment, learning control policy approximations. Importantly, this learning process enables the agent to handle stochastic events in the environments by exploring the state-control space using reward signals.

Our main contributions lie in three key areas. First, we enhance RANS [5], a simulator previously developed by our team, to accommodate more complex tasks and a diverse range of environment randomization profiles. Second, we demonstrate the high-performance capabilities of the Proximal Policy Optimization (PPO) [6] algorithm in both simulation and experimental scenarios. We evaluate its effectiveness in accomplishing three distinct tasks: navigating to a specific position, achieving a desired pose, and tracking a target velocity. Finally, we conduct a comprehensive comparison between the PPO-based approach and traditional optimal control algorithms, such as the Linear Quadratic Regulator (LQR), showcasing the benefits and drawbacks of the two methods under different environmental conditions.

Throughout this paper, we will refer to our robotic system, using Floating Platform (FP) and air-bearing platform interchangeably.

II. RELATED WORK

A. Floating Platforms control

Floating platforms are systems with air bearings attached to their lower surface. These bearings release pressurized air and create a thin film to levitate the platform, thereby counterbalancing its weight to produce a microgravity effect (in-plane components of gravity on the main body are negligible), thus emulating the drag-free and weightless environment of orbital spaceflight.

Recently, many research labs and organizations have focused on developing air bearings-based simulators with 3-DoF robotic systems [4], [7]–[14], making them the most popular testing facility to emulate microgravity on Earth.

To emulate mission scenarios for autonomous spacecraft tracking, servicing, rendezvous, and capture of a free-floating target, several works have further improved these platforms with 3-DoF robotic manipulators [9], [10], [15]. A typical approach for robotic arms mounted on air bearings platforms is to decouple the platform and the arm maneuvers. Sabatini et al. [9] focus on obtaining a coordinated maneuver in which the end effector moves thanks to the platform motion, hence optimizing fuel efficiency. They provide results both in simulation and on a real FP.

When focusing solely on the maneuvers of free-floating platforms, noteworthy developments have emerged. For instance, an innovative 3D-printed platform named “Slider” has been introduced [7]. Slider, equipped with eight thrusters, which can be precisely controlled through either motion in one of the 4 cardinal directions or 2 rotations. Furthermore, [8] presents an extensive characterization of air bearings platforms while also introducing a vision-based navigation system.

B. Deep Reinforcement Learning for thrust-based control

Over the past few years, there has been a flourishing utilization of ML and RL applied to space Guidance Navigation and Control (GNC) problems. These applications encompass a wide range of tasks, including planetary landing [16], path planning for lunar or asteroid hopping rovers [17], [18], spacecraft orbit control within unknown gravitational fields [19], and spacecraft map generation during orbits around small celestial bodies [20]. However, it is worth noting that most research employing deep reinforcement learning for aerospace control tasks shows simulation results.

To the best of our knowledge, only one prior work, namely [21], used reinforcement learning to guide both simulated and real-world floating platforms. In this paper, the authors combine DRL as a guidance policy whose trajectories are fed to a conventional controller to track. This work provides guidance techniques that successfully output velocity signals for the simulation and the experimental facility, achieving comparable performance to that observed during training.

Our work distinguishes itself from [21] in several key aspects. Firstly, we introduce a DRL agent capable of directly controlling the output thrust of the floating platform, eliminating the need for a separate trajectory tracker scheme. Secondly, our primary focus lies in delivering a comprehensive framework for training, assessing, and benchmarking DRL agents and optimal control methods across a spectrum of environmental conditions. These conditions represent a significant source of complexity when deploying AI agents on real systems, especially within the demanding space environment.

III. METHODS

A. Problem Formulation

We formulate the problem of controlling a FP’s maneuvers as a sequential decision-making task, wherein actions are selected to guide the system from an initial state to a target pose within a 2D space. The system considered in our experiments is a lightweight FP [22] developed at the University of Luxembourg. It is actuated by 8 “on-off thrusters” with a maximum thrust of 1N. The thrusters all share the same pressure line, such that when more than 1 thruster is fired, they all share equally the maximum available thrust. We consider a 10-dimensional state space defined as shown in Equation 1, where, at each time step t , θ represents the heading orientation, v_x and v_y are the linear velocities, ω_z is the angular velocity, tf denotes the task flag (integer to indicate which is the addressed task), and $td_{1-4} \in R$ include additional task-related data (such as distances to target position and target heading).

$$s_t = (\cos(\theta), \sin(\theta), v_x, v_y, \omega_z, tf, td_1, td_2, td_3, td_4) \quad (1)$$

The task-specific observations (to) are shown in Table I, where Δ denotes the distance between each variable (position, velocity or angle) and their target value. The observation space is structured as such so that this work can easily be extended to support multitask-capable policies. For the control of the platform, our agents use an 8-dimensional action space that corresponds to a binary activation of the available thrusters.

TABLE I: State task-specific observations

Task	tf	to ₁	to ₂	to ₃	to ₄
Go to position	0	Δx	Δy	-	-
Go to pose	1	Δx	Δy	$\cos(\Delta\theta)$	$\sin(\Delta\theta)$
Track velocity	2	Δv_x	Δv_y	-	-

To train our agents, we used the reward functions defined in (2, 3, 4). These rewards are shaped using an exponential term, as we empirically found that models trained with them converged faster while being more accurate.

- Go to position:

$$R = \exp\left(-\frac{e_p}{0.25}\right) - p \quad (2)$$

- Go to pose:

$$R = \exp\left(-\frac{e_p}{0.25}\right) \cdot S_p + \exp\left(-\frac{e_o}{0.25}\right) \cdot S_o - p \quad (3)$$

- Track velocity:

$$R = \exp\left(-\frac{e_v}{0.25}\right) - p \quad (4)$$

Here, the errors are considered as the absolute distance to the relative target. e_v is the velocity error, e_p and e_o are the position and orientation errors, and S_p and S_o their respective scaling coefficients. In our experiments, we set both S_p and S_o equal to 1. The quantity p stands for the possible three additional penalties, which can be added to penalize

energy consumption (high number of thrusters activation), high linear, and high angular velocities. We experimented with different penalty shapes and settled on using a linear penalty on the energy consumption as defined in (5).

$$p = 0.3 \sum_{i=1}^8 T_i \quad (5)$$

B. Simulation

Building upon our prior simulator RANS [5], we introduce enhancements to enable the platform to perform more complex tasks. RANS leverage Nvidia’s IsaacSim, specifically relying on OmniIsaacGym [23], a versatile simulator, capable of concurrently running thousands of environments. In the original RANS framework, only nominal system and environmental conditions were present, limiting the agents to learn on ideal conditions, which are usually far from those encountered when using the real FP systems. To mitigate this gap, we introduce RANS v2.0 which includes the following extensions: possibility to easily fine-tune the control policies through parameterized rewards and penalties, a disturbance generator that allows the injection of action and state noises, of a force and torque disturbance acting on the system, and a random thruster deactivation. RANS v2.0, with only approximately 10 minutes required to train a model on an RTX 4090, achieves a throughput of more than 40,000 steps per second with all disturbances enabled, which is very close to its previous version. Furthermore, it enables large-scale testing by swiftly evaluating thousands of initial conditions in seconds, provides extensive built-in examples and task sets. It offers rich visualization options, including metric tracking during training through the WandB API [24], and comprehensive evaluation metrics presented through tables and plots. The library uses the OpenAI Gym [25] format to define the RL loop, including the standard normalization of the observation space. Additionally, the integration of a ROS interface enhances the versatility of our framework, allowing easy integration and deployment of the control policies within real-world robotic systems.

C. Training Procedure

We reworked the PPO implementation from the RL Games library [26] as the foundation of our training procedure. This implementation utilizes GPU acceleration to vectorize observations and actions, facilitating efficient parallelization within the simulator by having both the physics simulation and the policy training residing on GPU. Our agents are designed as actor-critic networks with two hidden layers, each consisting of 128 units. They undergo training within their respective environments for a total of 2000 epochs or approximately 130M steps. For more details about the network or the PPO configuration, we invite the curious reader to refer to the training configuration files available along with the code release.

D. Benchmark comparison

In this paper, we aim to provide a benchmark comparison between deep reinforcement learning and optimal control

approaches, LQR in particular, for addressing the control problem of the floating platform in various scenarios. Our objective is not to establish the superiority of one method over the other, but rather to gain insights into the strengths and weaknesses of each approach under different environmental conditions and task requirements. To facilitate this comparison, we replicate the environment we had inside Isaac in MuJoCo [27]. We found MuJoCo more practical to evaluate the performance of traditional control algorithms, as it can be implemented easily without any parallelization or PyTorch dependencies. It also enabled us to test the policies outside the Omniverse environment and prepare for sim-to-real transfer. Our evaluation aims to provide insights into the relative strengths and weaknesses of RL and traditional control methods in our problem.

E. Optimal Controller

An infinite horizon discrete-time LQR controller [28] is used as a preliminary comparison with the DRL algorithm to control the FP. The position, linear velocities, orientation quaternions, and angular velocities in the 2D plane are considered as state variables of the system. The corresponding state matrices are calculated using finite differencing in MuJoCo so that they correspond to the control outputs from the eight thrusters. To account for the disturbances endured by the FP, the system matrices are updated at regular intervals.

F. Laboratory Experiment Setup

For real-world validation, we conducted experiments using the physical air bearings platform [22] located in the ZeroG Laboratory at the University of Luxembourg. This platform, with a weight of 5.32 Kg, radius and height of 31 and 45 cm, is equipped with a Raspberry Pi 4 for onboard control and interfacing. The ZeroG Lab contains an Optitrack Motion Capture System (MCS) that precisely tracks the platform’s pose at a high frequency of 200 Hz. From these measurements, we derive linear and angular velocities, which form the core components of the state representation required for policy inference. Our experimental setup maintains a connection between a laptop, the MCS, and the FP through a local network. The laptop serves as the ROS (Robot Operating System) master node of the network, subscribing to the Optitrack node to acquire pose data and publishing the actions of the trained agents at a rate of 5 Hz. This action frequency is deliberately constrained to prevent damage to the solenoid valves controlling the thrusters on the floating platform.

Figure 1 illustrates the key components interacting during the simulated training and validation phase (on the left), and those interacting during the closed-loop control tests of the real FP system in the Lab (on the right).

IV. EXPERIMENTAL SETUP

Our experiments encompass both simulation-based evaluations and real-world experimental validations.

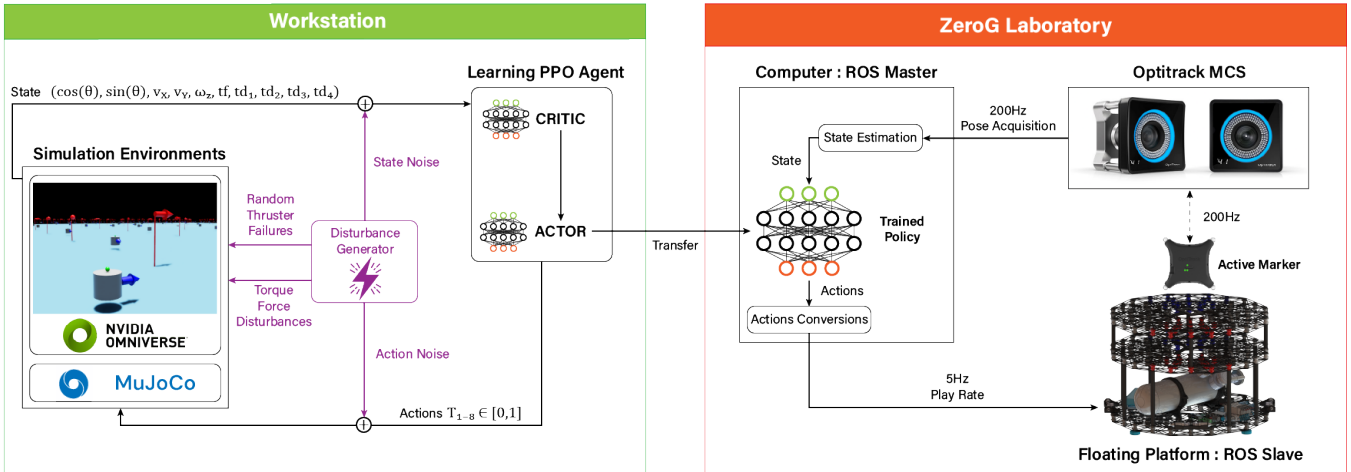


Fig. 1: Framework Employed for Training and Evaluation: On the left, we depict the agent’s interaction during both training and evaluation phases with the simulation environments, highlighting the incorporation of disturbances in the loop. On the right, we illustrate the deployment of the trained policy, while performing open-loop control on the real FP system.

A. Simulation-Based Evaluations

For the evaluation, each trained policy was tested across a diverse set of scenarios defined by various environmental conditions. The system and environmental disturbances are:

- Action Noise (AN): a random disturbance force of $\pm x$ N applied to every thruster;
- Velocity Noise (VN): $\pm x$ m/s added to the state velocities;
- Uneven Floor (UF): x N of force, added to simulate the floor unevenness, applied to the FP body throughout the episode, either with a constant direction or through a sinusoidal generated direction;
- Torque Disturbance (TD): x Nm of torque applied to the body’s center of mass;
- Random Thrusters Failure (RTF): a zeroing mask over the output actions to simulate one or multiple thruster failures which remains the same throughout the episode.

B. Tasks and Episodes

We define the different task as:

- Go to position: Starting from a random initial position in the plane, reach the given (x, y) coordinates;
- Go to pose: Starting from a random initial position in the plane, reach the given pose (position and orientation θ);
- Track velocity: Track the given velocity vector to follow a trajectory.

C. Performance Metrics

To evaluate the performance of policies, we employ 6 metrics for the position task and 9 for the pose task. For both the position and the pose, we record the percentage of the time the agent spends under a given distance threshold. For instance, PT_5 denotes the percentage of time spent under 5 cm, we also record this for 2 cm and 1 cm. This measure is also applied to the heading of the agents when performing the pose task. In this case, OT_5 is the percentage of time spent

under 5 degrees, this measure is also done for 2 degrees and 1 degrees. Finally, for both tasks, we also record the averaged linear (ALV) and angular velocities (AAV) as well as the average number of actions used per step (AAS).

D. Real-World Experimental Validations

To validate the transferability of the simulation-trained policies to the physical FP, we conducted real-world experiments using the laboratory setup described in section III-F. Five test runs were conducted for each policy, starting from different initial conditions. The variability in initial conditions includes random position and orientation. The same simulation task-specific metrics, including achieved accuracy, energy efficiency and trajectory smoothness, were employed.

V. RESULTS

Simulation-based experiments demonstrate the efficacy of the PPO-based approach in achieving the defined tasks. The agent exhibits rapid task completion, stability in control, and adaptation to various scenarios. Quantitative metrics and qualitative visualizations substantiate the agent’s high-performance capabilities.

A. Benchmark RL & LQR

In this section, we explore the behavior of an RL agent trained to perform the “go to pose” task, and compare it to the LQR controller. To characterize the controllers’ behaviors we expose them to a range of disturbances. Neither the RL agents nor the LQR are specifically adapted to incorporate methods from robust RL or robust optimal control theory. However, it should be noted that the RL agent was trained with some domain randomization to learn how to deal with force disturbances up to 0.25N. Both of them are evaluated in MuJoCo, with similarly randomized initial conditions. In Table II, each line corresponds to an experiment, with different disturbances being applied, and was acquired using 256 trajectories of 250 steps.

TABLE II: Benchmark of the RL model and LQR controller under disturbances. For PT and OT, higher is better. For ALV, AAV, and AAS lower is better. Colors in the table indicate the drop in performance relative to their own ideal conditions: blue(0-20%), green(20-40%), yellow(40-60%), red(60-80%), purple(80-100%). The parameters of the dynamics of the LQR are tuned without noise or disturbances enabled.

Conditions	Controllers	Disturbances					Metrics								
		AN (%)	VN (m/s)	UF (N)	TD (N/m)	RTF (-)	PT5 (%)	PT2 (%)	PT1 (%)	OT5 (%)	OT2 (%)	OT1 (%)	ALV (m/s)	AAV (rad/s)	AAS (-)
Ideal	RL	-	-	-	-	-	64	34	6	94	89	73	0.08	0.12	0.29
	LQR	-	-	-	-	-	73	41	17	27	11	5	0.07	0.16	0.10
Velocity Noise	RL	-	0.02	-	-	-	64	30	7	94	90	72	0.08	0.12	0.31
	RL	-	0.04	-	-	-	61	21	6	94	89	66	0.09	0.13	0.31
	LQR	-	0.02	-	-	-	53	21	6	4	1	0	0.09	0.49	0.23
	LQR	-	0.04	-	-	-	14	3	0	2	1	0	0.15	0.56	0.29
Constant Torque	RL	-	-	-	0.05	-	63	24	2	94	86	61	0.08	0.12	0.35
	LQR	-	-	-	0.05	-	57	20	6	3	1	0	0.07	0.43	0.35
Constant Force	RL	-	-	0.20	-	-	63	29	7	94	90	74	0.09	0.12	0.30
	RL	-	-	0.40	-	-	52	19	5	94	89	72	0.09	0.12	0.31
	LQR	-	-	0.20	-	-	66	17	4	28	12	6	0.07	0.15	0.12
	LQR	-	-	0.40	-	-	23	0	0	30	13	6	0.08	0.16	0.15
Constant Force & Torque	RL	-	-	0.20	0.05	-	62	24	5	94	86	61	0.08	0.12	0.35
	LQR	-	-	0.20	0.05	-	13	2	0	3	1	0	0.07	0.44	0.32
Thruster Failures	RL	-	-	-	-	1	32	15	6	70	55	36	0.10	0.12	0.28
	RL	-	-	-	-	2	15	6	2	45	31	20	0.16	0.15	0.25
	LQR	-	-	-	-	1	40	17	5	20	8	4	0.10	0.21	0.16
	LQR	-	-	-	-	2	12	4	1	11	4	2	0.14	0.28	0.22

First, the two test models are analyzed under ideal conditions with no disturbances. From the PT metrics, it is evident that the LQR controller converges faster in position with better accuracy than the RL, owing to substantially longer durations where the LQR maintains a position error under 1 cm. We can also see that the RL controller first aligns its heading with the goal, as it spends almost all its time under the 5° threshold. This is a byproduct of its reward shaping, which incentivizes the convergence of the heading as much as the position. Hence, to score the maximum of points, aligning the heading first is a sound strategy as it is the easiest under ideal conditions. Finally, AAS values show that the LQR is a lot more fuel efficient in these conditions, with 66% less fuel used than the RL agent.

When considering the Velocity Noise (VN), it is observed that with the lowest noise level, the RL performances remain unchanged, while the LQR is struggling, in particular with the attitude control. With 0.04 m/s of noise, the performance of both controllers decreases. Yet, the RL controller is more resilient than the LQR controller to this kind of disturbance, even though it was not trained for it. In the interest of brevity, we do not report action noise value in the table, as we found their effect to be negligible on both controllers.

Furthermore, when examining the Torque Disturbance (TD) of 0.05N/m, equivalent to 1/6-th of the total torque capacity of the platform, the performance of both controllers experiences a noticeable reduction; particularly, for the LQR controller. A similar pattern is observed with the force disturbance (UF), which would be equivalent to an uneven floor in the lab. In this case, we start by applying 0.2N of force on the platform, equivalent to 1/5-th of its maximum thrust. In this case, the performance of both controllers is close to the ideal conditions, with a small performance drop of the

LQR in fine positioning. When doubling it (0.4N), the RL policy remains close to its baseline, but the LQR performance decreases with it being unable to maintain positions under the 2.5cm threshold. Similar behaviors are observed upon the addition of both force and torque disturbances.

Finally, the thruster failures impact the performance of both controllers in the same manner. With a single failed thruster, both controllers perform relatively well, but the addition of a second thruster failure impedes the controller's ability to drive the FP to its defined goals.

Overall, while the LQR controller demonstrates greater efficiency and precision in position control with our current tuning, it encounters challenges when subjected to the selected range of disturbances. In contrast, RL exhibits a lower degree of energy conservation but offers stronger resilience when subject to a wide range of disturbances. It is possible that with a different cost function, better tuning of its weights, and a robust optimal control approach, the LQR becomes adept with these disturbances. Yet, the RL agent is not using a robust RL approach either, and domain randomization was only applied on force disturbances up to 0.25N which is less than the disturbances it can overcome.

B. ZeroG Laboratory

For experiments with the real FP system, we report two "go to pose" trajectories for both the RL and LQR methods. The controllers are run on the FP which is connected to a constant air supply through a tether. This tether applies some light unknown disturbances such as a small torque and force to the platform. Moreover, the system velocities are derived from the optitrack system. The observed velocities include a minor noise and experience small delays due to network communication.

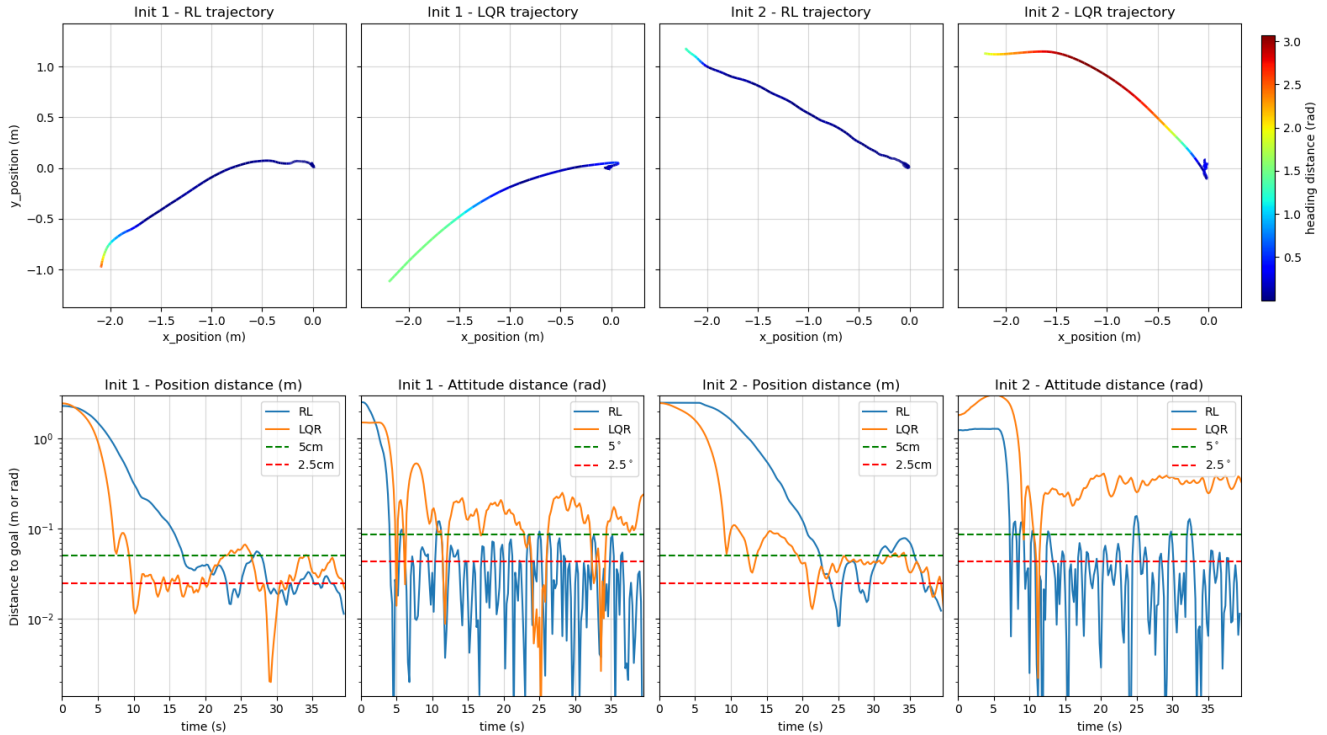


Fig. 2: Comparison of the RL and LQR controller on two different initial poses in the ZeroG lab. Init 1, denotes the first initial pose, Init 2 the second initial pose. For the trajectories, the scale of the y-axis is represented as a log value for better visualization.

Figure 2 illustrates the performance of each controller. The first row shows the trajectories of the FP, the second row the distance to the goal in position and in radiant. The first two columns have the rough same initial pose: Init1, while the two last share the same initial pose: Init2.

From the last row, it is evident that the LQR controller converges faster in position than the RL controller. This aligns well with the behaviors observed in the simulation benchmark, with an LQR controller converging faster. However, it is also apparent that the LQR solution exhibits a minor overshoot. Such an observation is also inline with the simulation benchmark, as the uneven floor in the lab likely disrupts the LQR controller by applying a subtle constant force, preventing it from reaching its simulation baseline performance. Looking at the top row, we can see that the LQR is also overshooting a bit. Of course, the behavior can be adjusted by modifying the weights associated with the importance of the error in position in the cost matrix. It is also worth noting that the LQR controller is sensitive to the weights; smaller weights do not incentivize the FP motion toward the goal. In comparison to the simulation, it was deemed necessary to alter the weights of the LQR controller to yield a more aggressive approach to achieve satisfying performances. As for the RL agent, it is noticeable that the FP initially aligns its heading and then gradually converges toward the goal. Consistently with the results from the simulation, the RL controller is significantly more

accurate in terms of heading while achieving a position accuracy similar to that of the LQR controller. Overall, both controllers performed well in the lab, reaching their expected performances.

VI. CONCLUSIONS

This study presents a comprehensive methodology for controlling a FP in 2D using deep reinforcement learning. The enhancements to our simulator extend its applicability, enabling the training of agents for complex tasks. The demonstrated effectiveness of the PPO algorithm, with seamless transfer behavior from the simulation to the FP system, highlights its potential for autonomous navigation in space. Furthermore, our comparison with traditional optimal control algorithms underscores the potential of the proposed approach in terms of absolute performance and especially when unknown stochastic events alter the environmental conditions.

In the future, we will experiment with more complex networks such as LSTMs or Transformers to see if they can cope better with the disturbances and in particular RTFs. We will also extend this framework to train agents to walk and jump in microgravity using a combination of leg motion and thrusters.

REFERENCES

- [1] J. Kopacz, R. Herschitz, and J. Roney, "Small satellites an overview and assessment," *Acta Astronautica*, vol. 170, pp. 93–105, 2020.
- [2] G. Curzi, D. Modenini, and P. Tortora, "Large constellations of small satellites: a survey of near future challenges and missions," *Aerospace*, vol. 7, p. 133, 2020.
- [3] M. B. Quadrelli, L. J. Wood, J. E. Riedel, M. McHenry, M. Aung, L. A. Cangahuala, R. Volpe, P. Beauchamp, and J. A. Cutts, "Guidance, navigation, and control technology assessment for future planetary science missions," *Journal of Guidance, Control, and Dynamics*, vol. 38, pp. 1165–1186, 2015.
- [4] T. Rybus and K. Seweryn, "Planar air-bearing microgravity simulators: Review of applications, existing solutions and design parameters," *Acta Astronautica*, vol. 120, pp. 239–259, 2016.
- [5] M. El-Hariry, A. Richard, and M. Olivares-Mendez, "Rans: Highly-parallelised simulator for reinforcement learning based autonomous navigating spacecrafts," 2023.
- [6] J. Schulman, F. Wolski, P. Dhariwal, A. Radford, and O. Klimov, "Proximal policy optimization algorithms," *arXiv preprint arXiv:1707.06347*, 2017.
- [7] A. Banerjee, S. Satpute, C. Kanellakis, I. Tevetzidis, J. Haluka, P. Bodin, and G. Nikolakopoulos, "On the design, modeling and experimental verification of a floating satellite platform," *IEEE Robotics and Automation Letters*, vol. 7, pp. 1364–1371, 2022.
- [8] Z. Huang, W. Zhang, T. Chen, H. Wen, and D. Jin, "Characterizing an air-bearing testbed for simulating spacecraft dynamics and control," *Aerospace*, vol. 9, p. 246, 2022.
- [9] M. Sabatini, P. Gasbarri, and G. B. Palmerini, "Coordinated control of a space manipulator tested by means of an air bearing free floating platform," *Acta Astronautica*, vol. 139, pp. 296–305, 2017.
- [10] L. Santaguida and Z. H. Zhu, "Development of air-bearing microgravity testbed for autonomous spacecraft rendezvous and robotic capture control of a free-floating target," *Acta Astronautica*, vol. 203, pp. 319–328, 2023.
- [11] S. Vyas, M. Zwick, and M. Olivares-Mendez, "Trajectory optimization and following for a three degrees of freedom overactuated floating platform," *2022 IEEE/RSJ International Conference on Intelligent Robots and Systems (IROS)*, 2022.
- [12] S. Kwok-Choon, K. Buchala, B. Blackwell, S. Lopresti, M. Wilde, and T. Go, "Design, fabrication, and preliminary testing of air-bearing test vehicles for the study of autonomous satellite maneuvers," in *Proceedings of the 31st Florida Conference on Recent Advances in Robotics, Orlando, FL, USA*, 2018, pp. 10–11.
- [13] C. Nieto-Peroy, G. Palmerini, E. J. de Oliveira, P. Gasbarri, M. Sabatini, and M. Milz, "Simulation of spacecraft formation maneuvers by means of floating platforms," in *2021 IEEE Aerospace Conference (50100)*, 2021, pp. 1–10.
- [14] J. D. Wapman, D. C. Sternberg, K. Lo, M. Wang, L. Jones-Wilson, and S. Mohan, "Jet propulsion laboratory small satellite dynamics testbed planar air-bearing propulsion system characterization," *Journal of Spacecraft and Rockets*, vol. 58, no. 4, pp. 954–971, 2021.
- [15] Y. Cao, S. Wang, X. Zheng, W. Ma, X. Xie, and L. Liu, "Reinforcement learning with prior policy guidance for motion planning of dual-arm free-floating space robot," *Aerospace Science and Technology*, vol. 136, p. 108098, 2023.
- [16] B. Gaudet, R. Linares, and R. Furfaro, "Deep reinforcement learning for six degree-of-freedom planetary landing," *Advances in Space Research*, vol. 65, no. 7, pp. 1723–1741, 2020.
- [17] X. Yu, P. Wang, and Z. Zhang, "Learning-based end-to-end path planning for lunar rovers with safety constraints," *Sensors*, vol. 21, p. 796, 2021.
- [18] T. Tanaka, M. Cescon, and H. A. Malki, "Linear quadratic tracking with reinforcement learning based reference trajectory optimization for the lunar hopper in simulated environment," *IEEE Access*, vol. 9, pp. 162 973–162 983, 2021.
- [19] S. Willis, D. Izzo, and D. Hennes, "Reinforcement learning for spacecraft maneuvering near small bodies," 2016. [Online]. Available: <https://api.semanticscholar.org/CorpusID:150378389>
- [20] D. M. Chan and A.-a. Agha-mohammadi, "Autonomous imaging and mapping of small bodies using deep reinforcement learning," in *2019 IEEE Aerospace Conference*, 2019, pp. 1–12.
- [21] K. Hovell and S. Ulrich, "On deep reinforcement learning for spacecraft guidance," *AIAA Scitech 2020 Forum*, 2020.
- [22] B. C. Yalçın, C. Martinez, S. Coloma, E. Skrzypczyk, and M. A. Olivares-Mendez, "Lightweight floating platform for ground-based emulation of on-orbit scenarios," *IEEE Access*, vol. 11, pp. 94 575–94 588, 2023.
- [23] V. Makoviychuk, L. Wawrzyniak, Y. Guo, M. Lu, K. Storey, M. Macklin, D. Hoeller, N. Rudin, A. Allshire, A. Handa *et al.*, "Isaac gym: High performance gpu-based physics simulation for robot learning," *arXiv preprint arXiv:2108.10470*, 2021.
- [24] L. Biewald, "Experiment tracking with weights and biases," 2020, software available from wandb.com. [Online]. Available: [https://www.wandb.com/\\$](https://www.wandb.com/$)
- [25] G. Brockman, V. Cheung, L. Pettersson, J. Schneider, J. Schulman, J. Tang, and W. Zaremba, "Openai gym," *arXiv preprint arXiv:1606.01540*, 2016.
- [26] D. Makoviichuk and V. Makoviychuk, "rl-games: A high-performance framework for reinforcement learning," May 2021. [Online]. Available: https://github.com/Denys88/rl_games
- [27] E. Todorov, T. Erez, and Y. Tassa, "Mujoco: A physics engine for model-based control," in *2012 IEEE/RSJ International Conference on Intelligent Robots and Systems*, 2012, pp. 5026–5033.
- [28] R. F. Stengel, *Optimal control and estimation*. Courier Corporation, 1994.